THE ASTROPHYSICAL JOURNAL, 453:727–740, 1995 November 10

WARM MOLECULAR GAS ASSOCIATED WITH COMETARY H II REGIONS

YOLANDA GÓMEZ,[1,2] GUIDO GARAY,[3] AND SUSANA LIZANO[2]
Received 1995 February 3; accepted 1995 May 22

ABSTRACT

We present observations of the $(J, K) = (2, 2)$ and (3, 3) inversion transitions of ammonia, made at $\sim 4''$ resolution with the VLA, in the direction of the G32.80+0.19 and G61.48+0.09 star-forming regions, which contain cometary-like and compact H II regions. Our data reveal the presence, in both complexes, of compact ammonia structures, with sizes of ~ 0.2 pc, which are intimately associated with the regions of ionized gas. The ammonia clumps have excitation temperatures in the range 60–80 K and molecular hydrogen densities in the range $(0.7–5) \times 10^4$ cm^{-3}. We suggest that these warm ammonia clumps correspond to compact molecular structures, embedded within more extended molecular clouds, which have been heated by the radiation from the star that ionizes the associated H II region and possibly compressed by the shocks driven by the expansion of the H II region.

We find that the molecular clumps associated with the cometary-like H II regions are located near the head of the ionized region and have line-center velocities similar to those of the ionized gas at the head position. These results imply that the cometary H II regions studied here, which exhibit strong gradients in the line-center velocities along their symmetry axis, are experiencing the champagne phase of evolution. In particular, the case of G61.48−0.09 is interesting because it seems that two champagne flows are occurring in this H II region. The ammonia clump associated with the most compact H II region within the G32.80+0.19 complex exhibits the (2, 2) main hyperfine (HF) line in absorption and the (3, 3) main HF line in emission, which we explain as due to a blend, within a synthesized beam, of an emitting region of hot molecular gas and an absorbing region of cold gas in front of a continuum source.

Subject headings: H II regions — ISM: individual (G32.80+0.19, G61.48+0.09) — ISM: molecules — radio lines: ISM — stars: formation

1. INTRODUCTION

Interferometric radio continuum observations have revealed that a high percentage of compact regions of ionized gas exhibit cometary morphologies (Wood & Churchwell 1989; Garay et al. 1993b; Kurtz, Churchwell, & Wood 1994; Miralles, Rodríguez, & Scalise 1994). Two main types of models have been proposed to explain this morphology: champagne flows and stellar wind bow shocks. In the champagne model the cometary shape is explained in terms of an ionized gas expanding in a medium with strong density gradients (Tenorio-Tagle 1979; Bodenheimer, Tenorio-Tagle, & Yorke 1979), while in the bow shock hypothesis it is explained as a bow shock produced by the stellar wind of an ionizing star that is moving supersonically through the ambient molecular cloud (Van Buren et al. 1990; Mac Low et al. 1991). The determination of the origin of cometary morphologies is an important task, since it would contribute either to the understanding of the characteristics and role of winds from massive stars cruising through molecular clouds, or, in the case that cometary regions truly mark the sites of newly formed massive stars, to determining the physical characteristics of the primordial medium.

In a previous work (Garay, Lizano, & Gómez 1994, hereafter GLG), we presented observations of the H92α radio recombination line made with high angular resolution toward the G32.80+0.19 and G61.48+0.09 complexes of ionized gas, both of which contain cometary-like H II regions. We found that the line-center velocities of the ionized gas within the cometary sources exhibit remarkable gradients along their axis of symmetry. The H92α line-center velocity smoothly increases from the head's leading edge to the tail's edge, by ~ 8 and 12 km s^{-1} for the G32.80+0.19 and G61.48+0.09 regions, respectively. We interpreted the observed kinematics as indicating that the cometary regions were undergoing champagne flows. Further support for this suggestion was provided by the presence, near the cometary regions, of compact and bright H II regions which are presumably embedded within the densest part of the inhomogeneous molecular medium. It would be unlikely to observe a moving bow shock cometary H II region associated with another H II region in a dense core (e.g., Fey et al. 1992). Although compelling, our observations did not provide a definite proof of the champagne hypothesis. In fact, we found that in the case of G32.80+0.19, the line width decreases along the symmetry axis, a feature predicted not in the champagne model but in the bow shock model.

The champagne model predicts that the ionized gas near the head of the cometary structure is at rest with respect to the molecular gas velocity (Yorke, Tenorio-Tagle, & Bodenheimer 1984), while the bow shock model predicts that it is moving with the velocity of the star (Van Buren & Mac Low 1992). Since the bow shock and champagne models make different predictions regarding the spatial and kinematical relationship between the ionized and molecular gas, a further key test that should be performed in order to distinguish clearly between them is to probe the physical conditions and kinematics of the molecular gas that immediately surrounds the cometary H II regions. Single-dish observations have already shown the presence of warm (above 50 K) and dense (over 10^5 cm^{-3}) molecu-

[1] National Radio Astronomy Observatory, P.O. Box 0, Socorro, NM 87801.
[2] Instituto de Astronomia, Universidad Nacional Autónoma de México, Apdo. Postal 70-264, 04510 México, D.F., México.
[3] Departamento de Astronomia, Universidad de Chile, Casilla 36-D, Santiago, Chile.

lar gas (Churchwell, Walmsley, & Cesaroni 1990; Plume, Jaffe, & Evans 1992) toward these H II complexes; however, their low spatial resolution did not allow the determination of the morphology of the dense molecular gas or of its location with respect to the ionized regions.

In this paper we report the results of high angular resolution observations, made with the VLA in the (2, 2) and (3, 3) inversion transition lines of ammonia, of the molecular gas toward the H II region complexes G32.80+0.19 and G61.48+0.09. Our main goals were to determine the kinematics and physical conditions of the dense and warm molecular gas present in these regions, to investigate its relationship to the cometary and/or compact H II regions, and to test whether or not the cometary H II regions are expanding in a medium with strong density gradients. Our ammonia observations toward these H II regions are reported in § 2. The main radio continuum and line results are presented in § 3. A derivation of the bulk physical parameters of the ammonia clouds, its physical association with the H II region, and a discussion of its kinematics are presented in § 4. Finally, we give our conclusions in § 5.

2. OBSERVATIONS

The observations were made on 1992 September 3 and 4 with the Very Large Array of the National Radio Astronomy Observatory.[4] The array was in the D configuration, with the shortest baseline being 40 m and the longest baseline 1000 m in length. This range of spacings gives an angular resolution of ~4″ and makes structures larger than about 60″ undetectable at 1.3 cm.

We observed the $(J, K) = (2, 2)$ and (3, 3) inversion transitions of the ammonia molecule in the spectral line mode toward the compact H II regions G32.80+0.19 and G61.48+0.09. We assumed rest frequencies of 23722.633 and 23870.129 MHz for the (2, 2) and (3, 3) transitions, respectively. We used a bandpass of 6.25 MHz, centered at an LSR velocity of 20 km s^{-1}, and 63 spectral channels 97.66 kHz wide each (~1.23 km s^{-1} at the observing frequencies) plus a continuum channel containing the central 75% of the total band. The (2, 2) and (3, 3) ammonia lines were observed simultaneously, with an LSR velocity coverage ranging from −18 to 58 km s^{-1}. The data were edited and calibrated in the standard manner using the Astronomical Image Processing System (AIPS) developed by the NRAO.

Flux densities were bootstrapped from observations of 1328+307, which was assumed to have a flux density of 2.4 Jy at 1.3 cm. The bandpass response was normalized using the observations of the bandpass calibrators 1226+023 and 0316+413. The solution obtained from self-calibration (Schwab 1980) of the data in the continuum channel was applied to the line channels. Line maps were made from the individual channel maps by subtracting a continuum map made from the average of the off-line channel maps. We made line maps using uniformly weighted (u, v) data with a Gaussian taper of 40 kλ which resulted in synthesized beams of ~4.″3 × 3.″7 and ~4.″3 × 3.″4 for the (2, 2) and (3, 3) transitions in the source G32.80+0.19, and ~3.″3 × 3.″3 for both transitions in G61.48+0.09. All spectra were Hanning smoothed to a velocity resolution of 2.46 km s^{-1}. The rms noise levels, after Hanning smoothing, in a single spectral line channel were ~4.6 and 4.5 mJy (beam solid angle)$^{-1}$ for the (2, 2) and (3, 3) observations of G32.80+0.19, and ~4.5 mJy (beam solid angle)$^{-1}$ for the (2, 2) and (3, 3) observations of G61.48+0.09.

[4] The National Radio Astronomy Observatory is operated by Associated Universities, Inc., under cooperative agreement with the National Science Foundation.

3. RESULTS

3.1. *Radio Continuum Emission*

Figure 1 shows the 1.3 cm self-calibrated maps of the radio continuum emission from complexes G32.80+0.19 and G61.48+0.09, made using the average of off-line channel maps from the (2, 2) and (3, 3) observations. At an angular resolution of ~4″, the G32.80+0.19 complex consists of two components: a bright and compact region located toward the southwest (component A) and an extended cometary-like

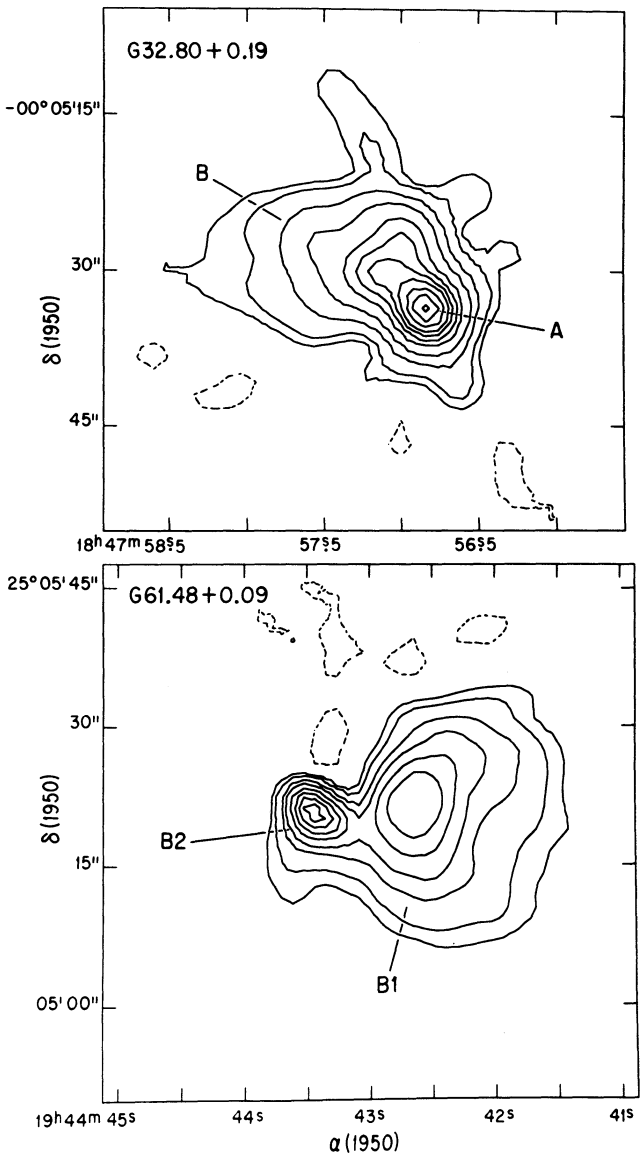

FIG. 1.—Radio continuum maps of H II region complexes at 1.3 cm. *Top:* G32.80+0.19 complex. Contour levels are −1, 1, 2, 5, 10, 20, 40, 50, 65, 80, and 95 percent of the peak flux density of 1.21 Jy beam^{-1}. The rms noise in the map is 2.5 mJy beam^{-1}, and the angular resolution is 4.″3 × 3.″7 at P.A. 63°. *Bottom:* G61.48+0.09 complex. Contour levels are −5, 5, 10, 20, 30, 45, 60, 75, and 90 percent of the peak flux density of 0.233 Jy beam^{-1}. The rms noise of the map is 2.7 mJy beam^{-1}, and the angular resolution is 3.″3 × 3.″3 at P.A. 45°.

region toward the northeast (component B). The G32.80+0.19 complex was previously mapped with the VLA at 2, 6, and 20 cm by Garay et al. (1993a), at 2 and 3.6 cm by Kurtz et al. (1994), and at 3.6 cm by GLG; in the latter paper the cometary morphology of component B is best distinguished. In the high angular resolution (~0".1) 2 cm map presented by Kurtz et al. (1994), component A appears resolved into two distinct components, while the emission from component B is only detected from the head structure.

At an angular resolution of ~4", the G61.48+0.09 (S88B) complex consists of two components: a bright and compact region toward the east (component B2) and an extended cometary-like region toward the west (component B1). Previous radio continuum interferometric observations toward the G61.48+0.09 complex were made at 6 cm by Felli & Harten (1981), at 6 and 20 cm by Garay et al. (1993b), and at 3.6 cm by GLG. The observed radio continuum parameters of the individual H II regions, derived from an average of the 23.7 and 23.9 GHz observations, are summarized in Table 1.

3.2. NH_3 *Lines*

As a result of the hyperfine interaction of the electric quadrupole moment of the nucleus with the electric field of the electrons, the (2, 2) and (3, 3) inversion lines of NH_3 are split into five components: a central main line, and two pairs of satellite lines separated symmetrically from the main line. In the absence of non-LTE effects and in the optically thin limit, the satellite lines should have an intensity of ~5% and ~3% of the main line for the (2, 2) and (3, 3) transitions, respecitvely.

3.2.1. *G32.80+0.19*

Toward the G32.80+0.19 region we detected the main hyperfine (HF) line of the (2, 2) and (3, 3) inversion transitions of ammonia, either in emission or in absorption. Line channel maps in the velocity range from 7.7 to 21.2 km s^{-1}, for the two transitions, are shown in Figure 2. From an inspection of this figure we distinguish three main features: (1) a northern component (G32.80 North), seen in the velocity range from 17.5 to 20.0 km s^{-1}, which appears in emission in both the (2, 2) and (3, 3) lines; (2) a middle component (G32.80 Middle), seen in the velocity range from 15.1 to 20.0 km s^{-1}, which appears in absorption in the (2, 2) line and in emission in the (3, 3) line; and (3) a southern component (G32.80 South), which appears in emission in the (3, 3) line (velocity range from 9.0 to 18.8 km s^{-1}) and in absorption in the (2, 2) line (velocity range from 13.8 to 18.8 km s^{-1}). These three components can be best appreciated in Figure 3, which shows contour maps of the velocity-integrated emission in the (2, 2) and (3, 3) transitions. Images of the velocity-integrated line emission, line-center velocity, and line width of the (2, 2) and (3, 3) transitions were obtained by computing moments of the line flux density using the AIPS task MOMNT.

TABLE 1

RADIO CONTINUUM PARAMETERS OF THE H II REGIONS[a]

SOURCE	POSITION[b] α(1950)	POSITION[b] δ(1950)	FLUX DENSITY (Jy)	DECONV. SIZE
G32.80+0.19A	$18^h47^m56^s.84$	−00°05′33″.5	1.6 ± 0.1	2″.0
G32.80+0.19B	18 47 57.08	−00 05 30.0	2.1 ± 0.2	7.3
G61.48+0.09B1	19 44 42.60	+25 05 21.6	2.5 ± 0.2	13
G61.48+0.09B2	19 44 43.44	+25 05 20.7	0.64 ± 0.04	4.1

[a] The parameters are an average of the values obtained from the 23.7 and 23.9 GHz maps.

[b] Peak position.

3.2.1.1. Sizes

The maps of the velocity-integrated emission in the main HF line of the (2, 2) and (3, 3) transitions (Fig. 3) show that the G32.80 North component has an elongated morphology oriented in a direction at ~25° east from north. From the (2, 2) map we measured deconvolved major and minor axes of 14".8 and 1".3, respectively, at P.A. 22°. From the (3, 3) map we measured deconvolved major and minor axes of 8".5 and 1".2, respectively, at P.A. 28°. The absorption features in the main HF line of the (2, 2) inversion transition from both the middle and south clumps are unresolved; we establish upper limits for their sizes of 2".0. The emission in the main HF line of the (3, 3) inversion transition from the Middle and South clumps taken together, arises roughly from an ellipse with deconvolved major and minor axes of 6".4 and 2".5, respectively, at P.A. 20°. Since these two clumps appear spatially blended, the determination of their individual sizes is, however, not straightforward. In what follows we will adopt for the G32.80 South clump a size of 2".5 (equal to the observed minor axis).

3.2.1.2. Center Velocities and Line Widths

The spectra of the (2, 2) and (3, 3) inversion transitions from each individual ammonia clump—integrated over their whole area of emission—are presented in Figure 4. This figure shows that the line-center velocity and line width of the emission (or absorption) from these clumps are distinctly different. In Table 2 we give the parameters of the NH_3 lines from each clump, determined by fitting a Gaussian profile to the corresponding spectrum. The average center velocity of the line emission from the G32.80 North cloud is 18.9 ± 0.2 km s^{-1} in the (2, 2) transition and 18.4 ± 0.3 km s^{-1} in the (3, 3) transition. For the G32.80 Middle cloud, the mean velocity of the (2, 2) absorption feature is 17.1 ± 0.3 km s^{-1}, while that of the (3, 3) emission feature is 14.9 ± 0.4 km s^{-1} (as will be discussed in § 4.1.2, these two features arise from two different physical regions). Toward the G32.80 South clump, the (3, 3; m) line is detected in emission over a broad velocity range (9–19 km s^{-1}), having an average center velocity of 14.1 ± 0.3 km s^{-1}. On the other hand, the (2, 2; m) line is seen weakly in emission at blueshifted velocities (8–13 km s^{-1}) and in absorption at redshifted velocities (14–19 km s^{-1}). From a Gaussian fit to the spectra observed at the peak position of the absorption feature we find a center velocity of 16.1 ± 0.2 km s^{-1}. The observed spectral appearance can be simply explained if there is a blend, within a synthesized beam, of an emitting region of hot molecular gas and an absorbing region of cold gas in front of a continuum source (see § 4.1.3).

Position-velocity diagrams, in the (2, 2) and (3, 3) lines, along a direction with a P.A. of 15° passing through the three ammonia clumps are shown in Figure 5. These diagrams were produced by averaging the emission over 4".8 wide strips; its position is illustrated with a solid line in Figure 3*a* (P.A. 15° through $\alpha = 18^h47^m57^s.06$ and $\delta = -00°05'21".5$). They clearly show the difference in the line-center velocities of the three ammonia clumps. Further, they show that the center velocity of the line emission across the G32.80 North clump is approximately constant, with a mean value of ~18.6 km s^{-1}. In addition, Figure 5 shows the remarkable broad width of the emission in the (3, 3) line from the G32.80 South clump.

The satellite lines were below the detection limits for all

1995ApJ...453..727G

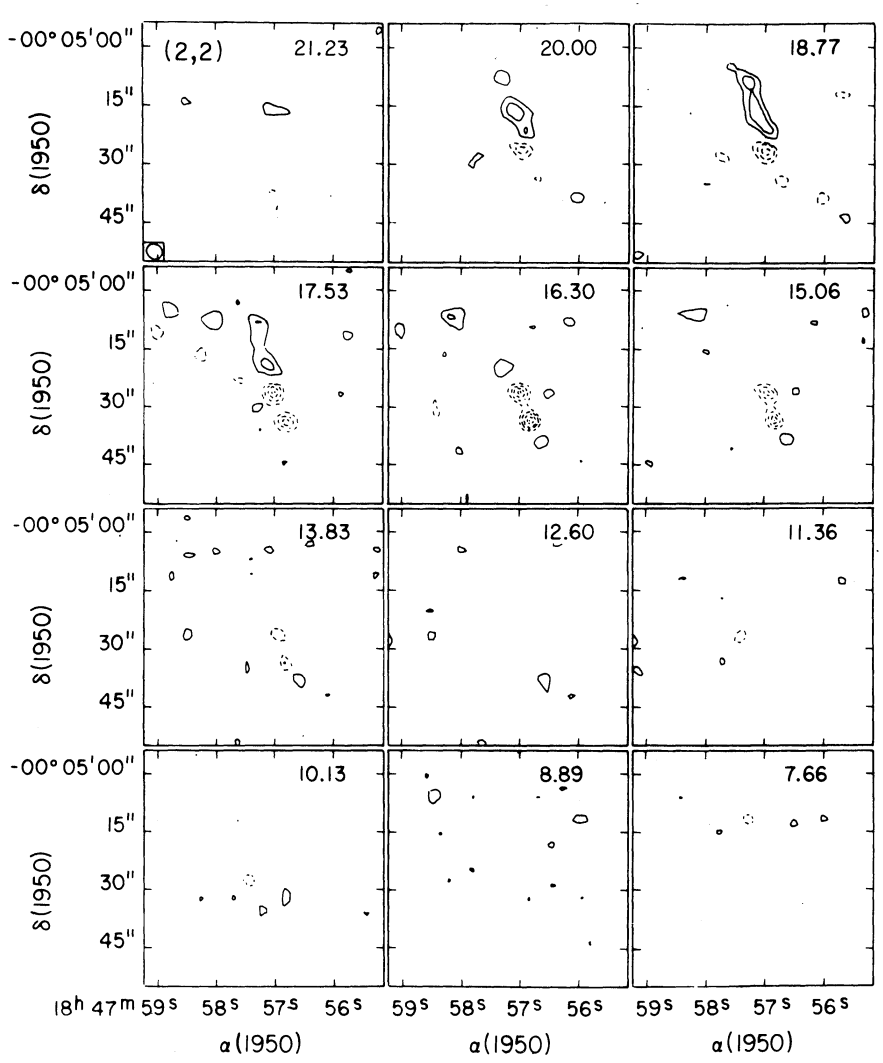

FIG. 2a

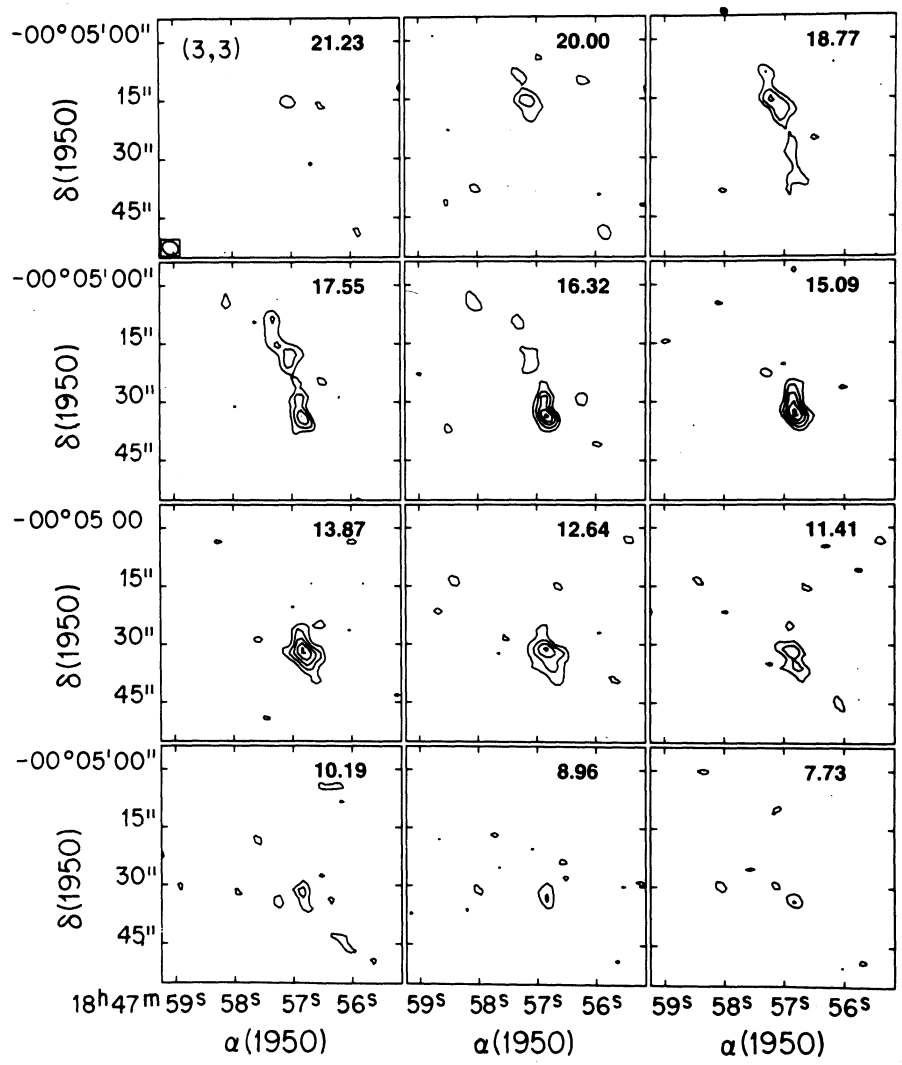

FIG. 2b

FIG. 2.—Channel maps of inversion transition lines of ammonia toward the G32.80+0.19 region. (*a*) (2, 2) transition. Contour levels are (−11, −9, −7, −5, −3, 3, 5, 7, and 9) × 4.6 mJy beam^{-1}, the rms noise of the maps. (*b*) (3, 3) inversion transition. Contour levels are (3, 3, 5, 7, 9, and 11) × 4.5 mJy beam^{-1}, the rms noise of the maps.

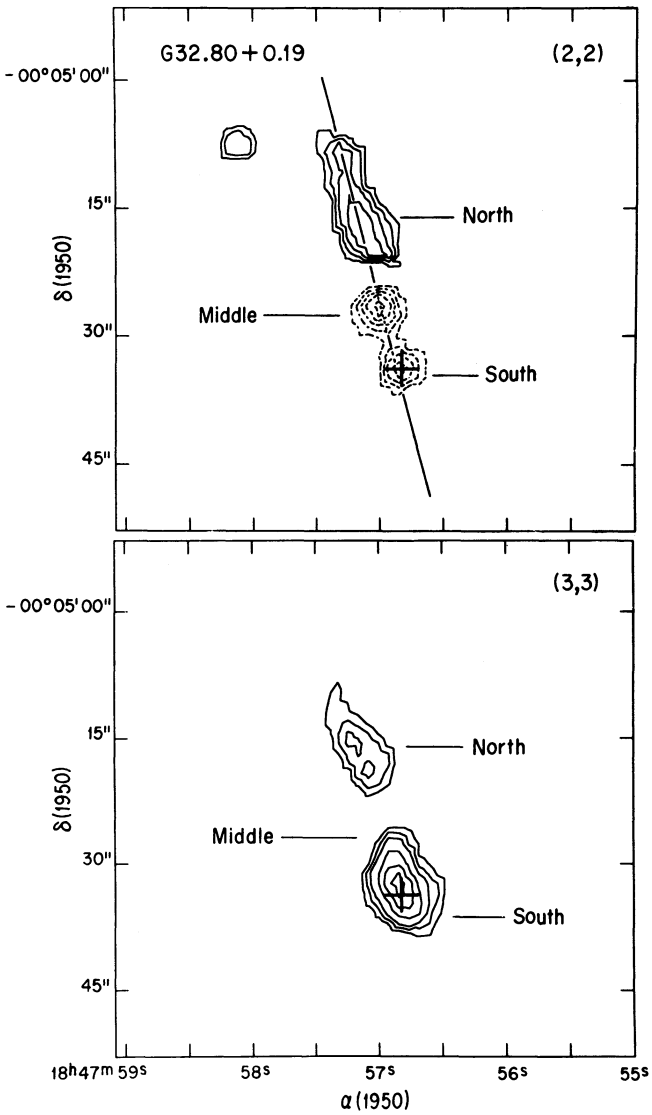

FIG. 3.—Maps of the velocity-integrated emission/absorption from the G32.80+0.19 ammonia clumps. *Top:* (2, 2) line. Contour levels are (−9, −7, −5, −3, −1, 1, 2, 3, and 4) × 21 mJy beam^{-1} km s^{-1}. *Bottom:* (3, 3) line. Contour levels are (−1, 1, 2, 3, 5, 7, and 9) × 37 mJy beam^{-1} km s^{-1}. The cross indicates the peak position of the radio continuum source A, taken from Garay, Lizano, & Gómez (1994).

three ammonia clumps. Upper limits for the flux densities per beam in the (2, 2) and (3, 3) satellite lines were determined from maps made averaging the line channel maps at the velocities expected for the satellite lines. Upper limits (3 σ) for the emission in the (2, 2) and (3, 3) satellite lines are 9.9 and 10.2 mJy beam^{-1} for G32.80 North, 9.9 and 9.3 mJy beam^{-1} for G32.80 Middle, and 10.5 and 10.2 mJy beam^{-1} for G32.80 South, respectively. These upper limits imply opacities in the main HF line of less than ~ 10 for each of the components.

3.2.2. *G61.48+0.09*

Toward the G61.48+0.09 region, emission in the main HF line was clearly detected in the (3, 3) inversion transition but barely detected in the (2, 2) inversion transition. Figure 6, which presents line channel maps of the (3, 3) observations in the velocity range from 16.3 to 26.1 km s^{-1}, shows that emission is detected in the velocity range from 20.0 to 22.5 km s^{-1}. Images of the velocity-integrated line emission, line-center velocity, and line width were obtained by computing moments of the line flux density using the AIPS task MOMNT. The map of the velocity integrated emission in the (3, 3) line, presented in Figure 7, shows that the emission arises from two main regions: a western component (G61.48 West), associated with the cometary H II region (B1), and an eastern component (G61.48 East), associated with the compact H II region (B2). We roughly estimated a deconvolved angular size $\leq 3''$ for G61.48 East and $\sim 3''$ for G61.48 West.

3.2.2.1. Center Velocities and Line Widths

The spectra of the (3, 3) inversion transition from the G61.48 East and G61.48 West clumps, integrated over their whole area of emission, are shown in Figure 8. The parameters of the NH_3 lines from each clump, determined by fitting a Gaussian profile to the corresponding spectra, are given in Table 2. The average center velocity of the line emission from the G61.48 West and G61.48 East clumps are 21.6 ± 0.2 km s^{-1} and 21.9 ± 0.2 km s^{-1}, respectively. The absence of (or very weak) emission in the (2, 2) main line but relatively strong emission in the (3, 3) main line from these clumps can be simply explained if the emission arises from a hot, optically thin, ammonia gas (see § 4.2.1).

A position-velocity diagram of the emission in the (3, 3) line, along a direction with a P.A. of 90° passing through the two ammonia clumps, is shown in Figure 9. This diagram was produced by averaging the emission over 6″.0 wide strips, whose central position is illustrated with a solid line in Figure 7*b* (δ = 25°05′21″.2). Figure 9 shows that the line-center veloc-

TABLE 2

AMMONIA LINE PARAMETERS

FEATURE	TRANSITION	POSITION[a] α(1950)	POSITION[a] δ(1950)	V_{LSR} (km s^{-1})	ΔV (km s^{-1})	TOTAL FLUX DENSITY (mJy)	Θ_s[b] (″)
G32.80 North.....	(2, 2; m)	18h47m57s.15	−00°05′17″.2	18.9 ± 0.2	3.1 ± 0.4	166 ± 18	4.4
	(3, 3; m)	18 47 57.07	−00 05 18.3	18.4 ± 0.3	4.8 ± 0.7	129 ± 17	3.2
G32.80 Middle.....	(2, 2; m)	18 47 57.00	−00 05 26.5	17.1 ± 0.3[c]	5.4 ± 0.8	−52 ± 6	≤2
	(3, 3; m)	18 47 56.88	−00 05 28.8	14.9 ± 0.4[d]	6.5 ± 0.9	50 ± 6	∼2
G32.80 South	(2, 2; m)	18 47 56.81	−00 05 33.5	16.1 ± 0.2[c]	3.5 ± 0.5	−57 ± 17	≤2
	(3, 3; m)	18 47 56.78	−00 05 32.5	14.1 ± 0.3[d]	7.1 ± 0.8	143 ± 14	∼2.5
G61.48 East (B2)	(3, 3; m)	19 44 43.41	+25 05 20.1	21.9 ± 0.2	3.5 ± 0.5	60 ± 7	∼1.5
G61.48 West (B1).....	(3, 3; m)	19 44 42.76	+25 05 19.4	21.6 ± 0.2	4.2 ± 0.4	73 ± 6	∼3

[a] Peak position.
[b] Geometric mean of angular sizes.
[c] Absorption feature.
[d] Emission feature.

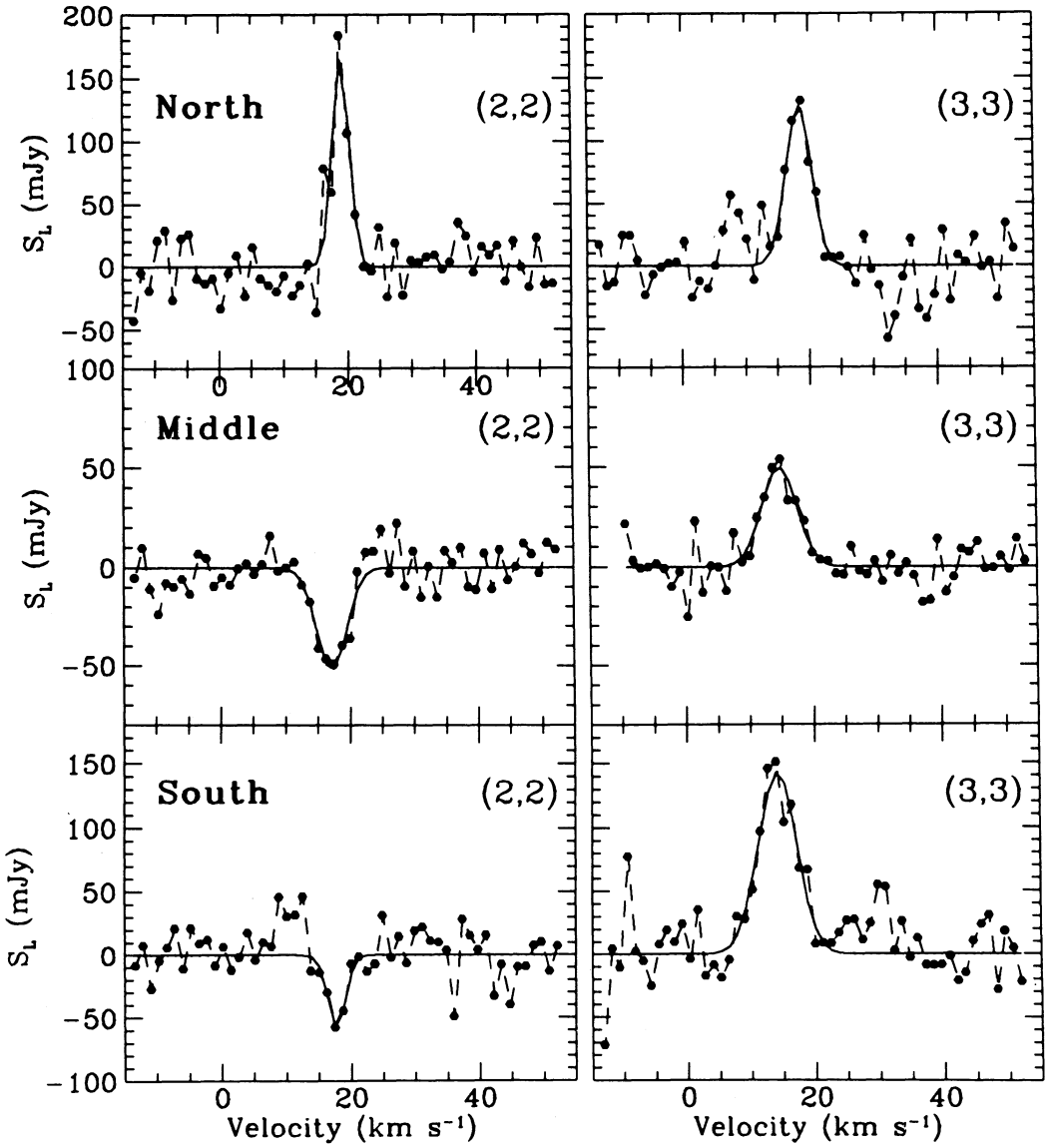

FIG. 4.—Integrated spectra in the (2, 2) and (3, 3) lines of NH_3 from the G32.80+0.19 molecular clumps. *Top:* G32.80 North. *Middle:* G32.80 Middle. *Bottom:* G32.80 South.

ity of the emission from G61.48 West is approximately constant across the source, having an average value of 22 km s^{-1}, similar to the line-center velocity of the G61.48 East clump. It also shows that the line widths of these ammonia components are ~3.8 km s^{-1}, similar to the average line width, in the (2, 2) transition, of a large sample of ammonia clouds associated with compact H II regions, of ~3.4 km s^{-1} (Churchwell et al. 1990).

The satellite lines were not detected toward the G61.48+0.09 region. Upper 3 σ limits to the flux densities per beam in the satellite lines, determined by averaging the emission in the three channel maps where the satellite lines were expected, are 3.2 and 3.5 mJy beam^{-1} respectively for the (2, 2) and (3, 3) transitions toward the G61.48 West region, and 3.5 mJy beam^{-1} for the (3, 3) transition toward the G61.48 East region. These upper limits imply opacities in the main HF line of less than 15 for each component.

4. ANALYSIS AND DISCUSSION

In what follows we derive the bulk physical parameters of the ammonia clumps observed toward the two H II region complexes. The derived parameters are summarized in Table 3.

4.1. *G32.80+0.19 Ammonia Clumps*

From single-dish CO observations, Kurtz et al. (1995) determined that the radial velocity of the G32.80+0.19 ambient molecular cloud is 16.3 ± 0.05 km s^{-1}. This velocity is in good agreement with the average line-center velocity of the NH_3 emission in the (1, 1) and (2, 2) inversion transitions, measured with single-dish (FWHM = 40″), of 16.1 ± 0.5 km s^{-1} (Churchwell et al. 1990). In the following discussion we will assume that the G32.80+0.19 ambient cloud has a rest velocity of 16.3 km s^{-1} and that it is at the far kinematical distance of 13 kpc (Churchwell et al. 1990).

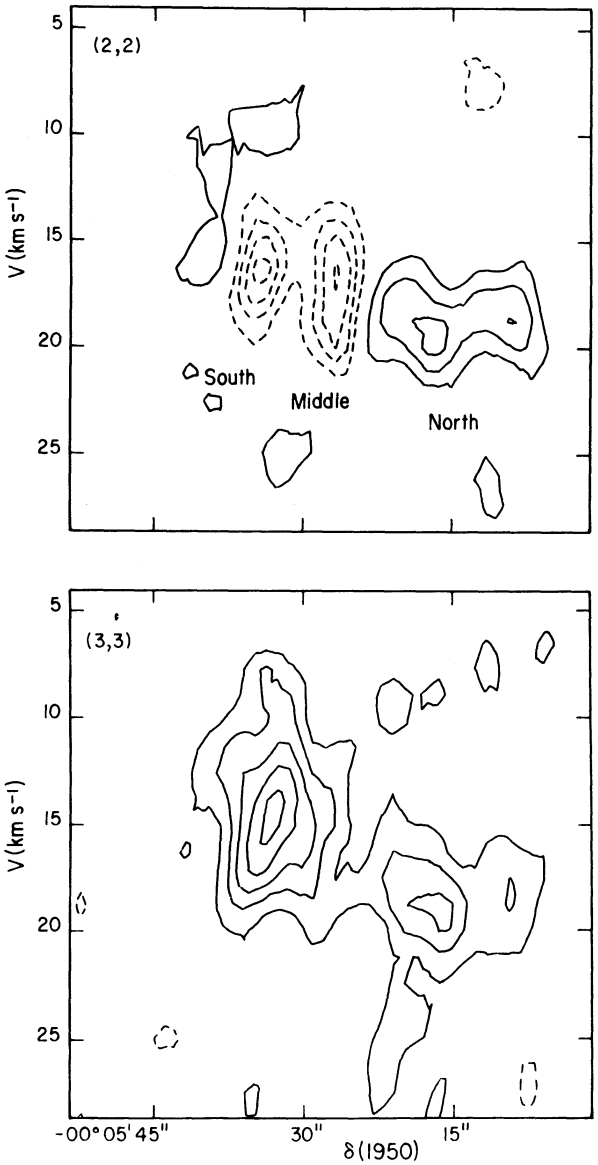

FIG. 5.—Position-velocity diagrams of the NH_3 emission/absorption from the G32.80+0.19 region along a direction (shown in Fig. 3) at P.A. 15° passing through $\alpha = 18^h47^m57^s.06$, $\delta = -00°05'21''.5$. *Top:* (2, 2) line. Contour levels are (−4, −3, −2, −1, 1, 2, and 3) × 8 mJy beam^{-1}. *Bottom:* (3, 3) line. Contour levels are (−1, 1, 2, 3, 4, and 5) × 8 mJy beam^{-1}.

4.1.1. *G32.80 North*

Toward the G32.80 North clump, both the (2, 2) and (3, 3) main lines appear in emission (see Figs. 2 and 3) which allows us to estimate its rotational temperature. Assuming an LTE ortho-para ratio for the NH_3 molecule and assuming that the emission is optically thin, we can estimate an average rotational temperature from the ratio of the (3, 3) and (2, 2) lines:

$$T_{\rm rot}(33-22) = 59.6\left[\ln\left(3.5\,\frac{S_L(2,2;\,\mathrm{m})\Delta v(2,2;\,\mathrm{m})}{S_L(3,3;\,\mathrm{m})\Delta v(3,3;\,\mathrm{m})}\right)\right]^{-1}\ \mathrm{K}\,, \quad (1)$$

where $S_L(J, K;\,\mathrm{m})$ and $\Delta v(J, K;\,\mathrm{m})$ are, respectively, the flux density and the line width of the main line of the (J, K) inversion transition. Using the velocity-integrated flux density over a region where the emission in the two transitions overlaps we derive an average rotational temperature of $\sim 56 \pm 14$ K. We note that the same temperature is derived using the parameters given in Table 2.

An estimate of the optical depth in the line, τ_L, can be obtained from the peak brightness temperature of the line once the continuum has been subtracted, T_L^b, using the expression

$$T_L^b = (T_{\rm ex} - T_{\rm bg})(1 - e^{-\tau_L})\,, \quad (2)$$

where $T_{\rm ex}$ is the excitation temperature of the line and $T_{\rm bg}$ is the brightness temperature of a background source. The peak line brightness is computed from the observed peak flux density per beam, S_L (in mJy), using the expression $T_L^b = A(S_L/\theta_b^2)$, where θ_b is the FWHM beam size (in arcseconds). Assuming that the intensity of the line is uniform within the beam, the constant A takes the values of 3.15 and 3.11 for the (2, 2) and (3, 3) transitions, respectively. The peak brightness temperature in the (3, 3) line is 8.3 K. Adopting $T_{\rm bg} \simeq 2.7$ K, since the ammonia G32.80 North structure does not appear projected toward a radio continuum source at 1.3 cm, and assuming $T_{\rm ex} = T_{\rm rot} = 56$ K, we find that the opacity in the main line of the (3, 3) transition is ~ 0.17.

The total column density of NH_3 can be computed from the optical depth $\tau(J, K)$ and $T_{\rm rot}$, assuming an LTE population for all ammonia levels, using the relation

$$N(\mathrm{NH_3}) = \frac{1.65 \times 10^{14} J(J+1)}{\nu g_K K^2 (2J+1)}\,\Delta v \times \tau(J, K) Q T_{\rm ex} \exp\left[\frac{E(J, K)}{kT_{\rm rot}}\right], \quad (3)$$

where ν is the transition frequency in gigahertz, g_K is the sta-

TABLE 3

DERIVED PARAMETERS OF THE AMMONIA STRUCTURES

Feature	l (pc)	T (K)	$N(\mathrm{NH_3})$ ($\mathrm{cm^{-2}}$)	$n(\mathrm{H_2})^a$ ($\mathrm{cm^{-3}}$)	$M(\mathrm{H_2})$ ($M_\odot$)	L_* ($\times 10^5\ L_\odot$)
G32.80 North	0.24	56 ± 14^b	5×10^{15}	7×10^3	10	6.2[c]
G32.80 South	0.16	60 ± 10^d	3×10^{16}	5×10^4	18	3.5
G61.48 West (B1).....	0.08	80 ± 15^d	1×10^{16}	4×10^4	2	2.5
G61.48 East (B2)	0.07	70 ± 15^d	6×10^{15}	3×10^4	0.6	0.7

[a] Assuming an $[\mathrm{H_2/NH_3}]$ abundance ratio of 10^6.
[b] Rotational temperature.
[c] G32.80+0.19 B H II region.
[d] Excitation temperature.

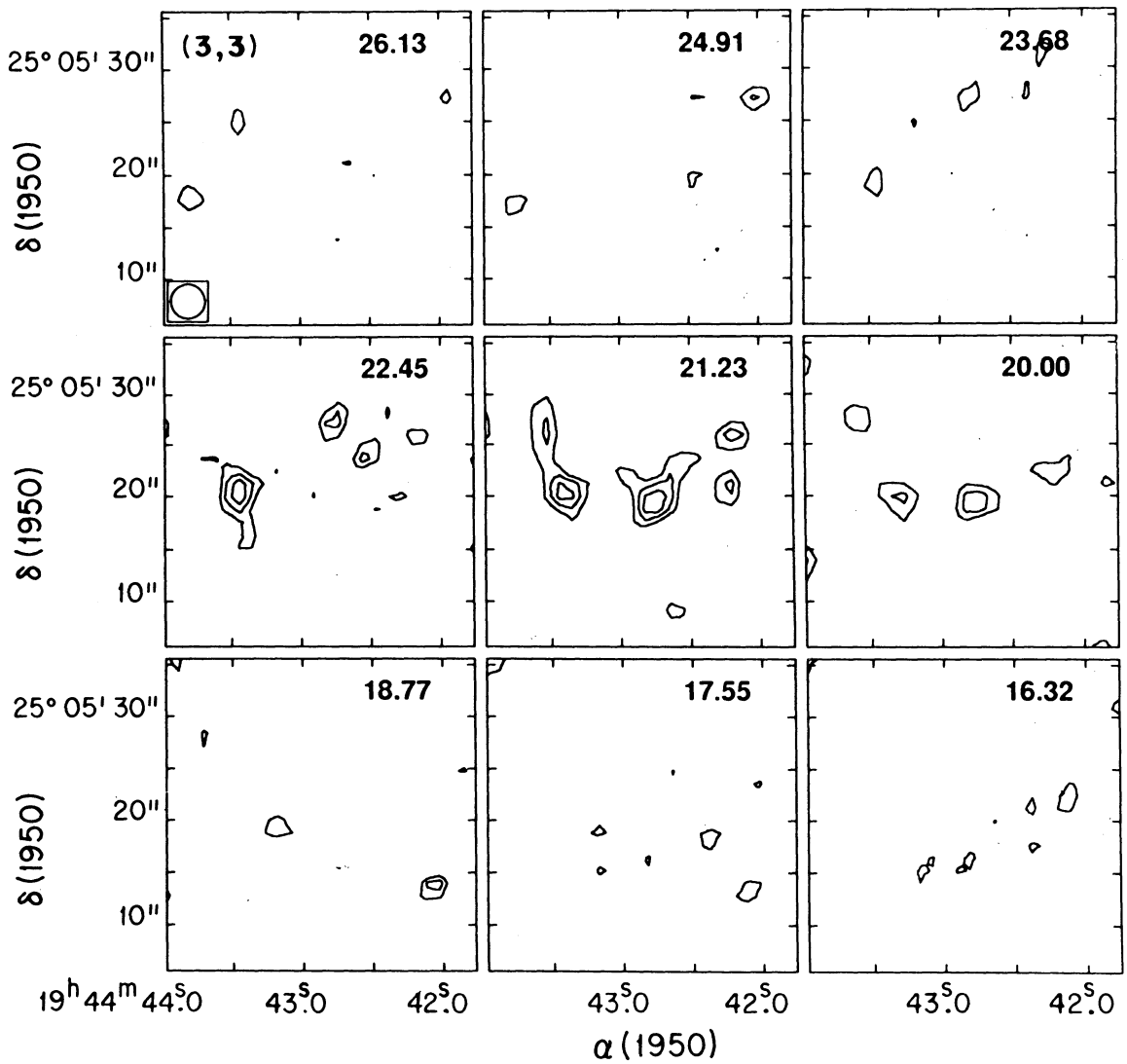

FIG. 6.—Channel maps of the (3, 3) inversion transition lines of ammonia toward the G61.48 + 0.09 region. Contour levels are (−5, −4, −3, 3, 4, 5, and 6) × 4.5 mJy beam^{-1}, the rms noise of the maps.

tistical weight ($g_K = 2$ for the ortho states), $E(J, K)$ is the rotational energy of the (J, K) level above the ground state, Δv is the line width in kilometers per second, Q is the partition function, and k is Boltzmann's constant. Assuming LTE, and for $T_{\rm rot} \gg 20$ K, we can use the partition function given by (e.g., Genzel et al. 1982)

$$Q = 115\left(\frac{T_{\rm rot}}{200\ {\rm K}}\right)^{3/2}.$$

Using $\tau(3, 3) = 1.12\tau(3, 3; {\rm m})$, $T_{\rm ex} \simeq T_{\rm rot} = 56$ K, and $\Delta v = 3.1$ km s^{-1}, we obtain a total column density of ammonia of $\sim 5 \times 10^{15}$ cm^{-2}.

The ammonia density can be derived from the column density by dividing by a characteristic length. Assuming a path length of 0.24 pc, which corresponds to the geometrical mean of the observed projected linear sizes, and assuming an $[H_2/NH_3]$ abundance ratio of 10^6, we obtain a molecular hydrogen density of 7×10^3 cm^{-3}. In addition, since the NH_3 lines are optically thin, the mass of molecular gas can be derived from the observed parameters in a single transition. In terms of the flux density and the line width of the (3, 3; m) line, using expression (2) of Garay, Moran, & Rodríguez (1993a), with $T_{\rm ex} \simeq T_{\rm rot} \simeq 56$ K, $[H_2/NH_3] = 10^6$, we derive a molecular mass for G32.80 North of $\sim 10\ M_\odot$.

The G32.80 North clump is located just beyond, and roughly following, the northwestern edge of the cometary H II region. This can be appreciated in Figure 10, which shows a map of the velocity-integrated emission (zero-order moment) in the (3, 3) line superposed on a contour map of the radio continuum emission at 8.3 GHz taken from GLG. These characteristics suggest that the G32.80 North cloud may be part of the edge delineating the dense molecular wall that confines the ionized champagne flow from the associated H II region (see discussion below).

4.1.2. *G32.80 Middle*

The G32.80 Middle clump shows the (2, 2) line in absorption and the (3, 3) line in emission. The absorption feature is found projected right on top of the head of the cometary region of

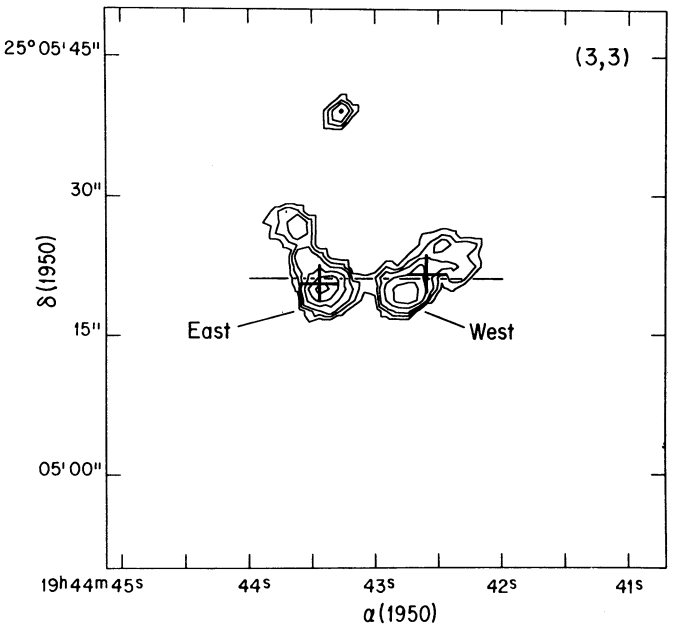

FIG. 7.—Maps of the (3, 3) line velocity integrated emission from the G61.48+0.09 region. Contour levels are (−1, 1, 2, 3, 5, 7, and 9) × 8.2 mJy beam^{-1} km s^{-1}. The crosses indicate the peak positions of the radio continuum sources B1 and B2, taken from Garay et al. (1994).

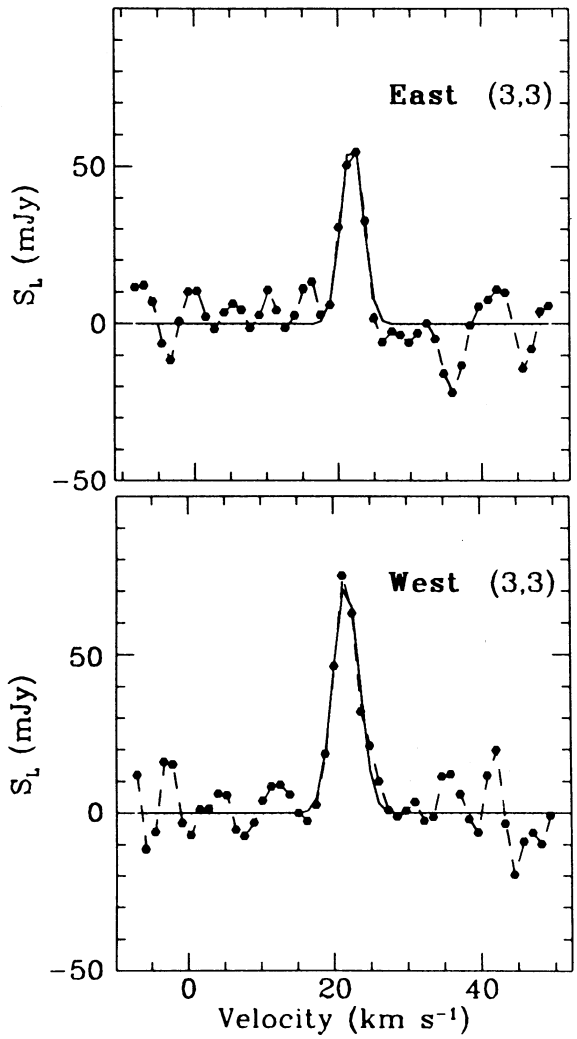

FIG. 8.—Integrated spectra in the (3, 3) line of NH_3 from the G61.48+0.09 molecular clumps.

ionized gas, and has a radial velocity of ~17 km s^{-1} (see Table 2). The (3, 3) emission component is slightly displaced toward the west and has a velocity of ~15 km s^{-1}. Its eastern edge closely follows the head of the cometary region of ionized gas. The fact that absorption is seen only in the (2, 2) line, and not in the (3, 3) line, suggests that the absorption arises in a cold molecular gas between the observer and the region of ionized gas (see discussion in § 4.1.3). Note that the velocity of the (2, 2) absorption feature is close to the systemic velocity of the ambient molecular cloud.

GLG showed that the velocity of the ionized gas from the cometary region exhibits a remarkable gradient along its symmetry axis. The velocity increases from ~14 km s^{-1} at the head's leading edge to ~22 km s^{-1} toward the tail. The observed morphology and velocity field of the ionized gas and associated molecular gas strongly suggest that the cometary H II region is undergoing a champagne flow. The ammonia emission in the (3, 3) line from the whole region line indicates that the density of the molecular cloud is increasing in the southwest direction. The ionized gas is flowing, away from the observer, in the direction of the decreasing density gradient. We suggest that the (3, 3) ammonia emission from G32.80 Middle arises in the postshock layer of warm gas left behind by the shock driven by the expansion of the H II region into the molecular cloud. The velocity of the (3, 3) line is similar to the velocity of the ionized gas at the head position, as expected in the champagne model. The broad observed line width, of ~6.5 km s^{-1}, probably reflects the motions of the shocked gas velocities along the line of sight. In support of this shock hypothesis, Hofner & Churchwell (1995) detected several H_2O masers spatially associated with this and the G32.80 North ammonia components. We note that since the (2, 2) line, detected in absorption, and the (3, 3) line, detected in emission, arise from slightly displaced regions, it was not possible to estimate the exctitation temperature of the ammonia transitions, and therefore we could not compute physical parameters for this cloud, such as its density and molecular mass.

4.1.3. *G32.80 South*

Toward the G32.80 South clump the main HF line of the (2, 2) inversion transition appears mainly in absorption, while the main HF line of the (3, 3) inversion transition is seen in emission; thus equation (1) cannot be used to derive the rotational temperature of this cloud. Nevertheless, in this case, the appearance of the observed spectra suggests that there is a blend, within a synthesized beam, of an emitting region of hot molecular gas and an absorbing region of cold gas in front of a continuum source (cf. Garay & Rodríguez 1990).

The excitation temperature of the warm ammonia gas can be obtained by fitting the observed spectra in the (2, 2) and (3, 3) lines, using a simple model like that developed by Garay & Rodríguez (1990), in which cold and hot components of molecular gas are seen along the line of sight toward a continuum radio source, but also taking into account the absorption of the emission from the hot cloud by the cold cloud. In this model, which assumes that the clouds have constant excitation conditions, the line brightness temperature at radial velocity v, $T_L(v)$,

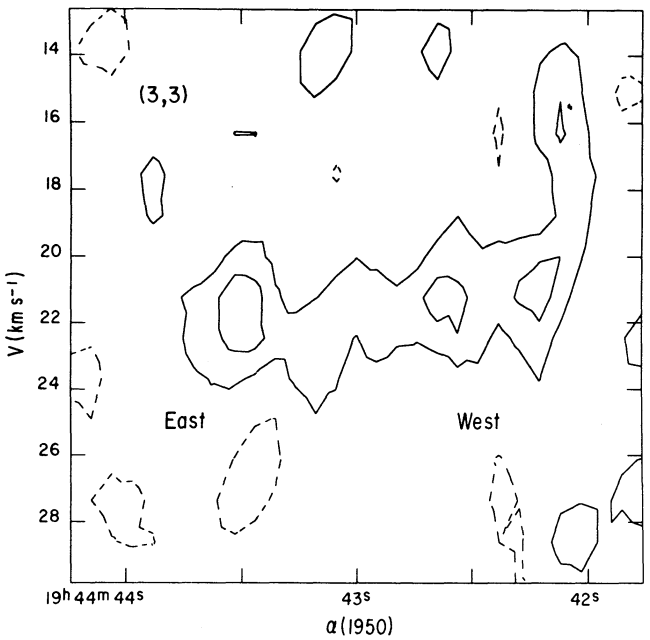

FIG. 9.—Position-velocity diagram of the (3, 3) NH_3 emission from the G61.48+0.09 region along a direction passing through the two ammonia clumps (P.A. 90°, $\delta = 25°05'21''.2$; see Fig. 7).

is given by

$$T_L(v) = (T_H f_H - T_0 X_{0H})(1 - e^{-[\tau_H(v) + \tau_C(v)]}) + (T_C f_C - T_H f_H - T_0 X_{0C} + T_0 X_{0H})(1 - e^{-\tau_C(v)}), \quad (4)$$

where T_H and T_C are the excitation temperatures, f_H and f_C the beam filling factors, and $\tau_H(v)$ and $\tau_C(v)$ the optical depths, at velocity v, of the hot and cold molecular gas, respectively. Further, f_0 is the beam filling factor of the continuum source, T_0 is the beam-averaged continuum brightness temperature, and X_{0H} and X_{0C} are the fractions of the H II region covered by the hot and cold gas, respectively.

Figure 11 presents the spectra in the (2, 2) and (3, 3) transitions observed at the position of the peak absorption feature in the (2, 2) line ($\alpha = 18^h47^m56^s.810$; $\delta = -00°05'33''.54$). At this position, which coincides with the peak position of the compact region of ionized gas (component A in Fig. 1), the brightness temperature in the (2, 2) line is −13.2 K, the brightness temperature in the (3, 3) line is 12.1 K, and the brightness temperature of the radio continuum emission at 1.3 cm is T_0 = 233 K. Since we do not observe appreciable absorption in the NH_3 (3, 3) line, it suggests that the hot gas covers a small fraction of the radio continuum source. The continuous lines in Figure 11 represent the model spectra that best fitted the observed spectra. Fixed parameters in the model, taken directly from our observations, are, for the hot cloud, a line-center velocity of 14.1 km s^{-1} and a line width of 7.1 km s^{-1}; for the cold cloud, a line-center velocity of 16.3 km s^{-1}, a line width of 3.5 km s^{-1}, and $T_C \simeq 15$ K (S. Kurtz 1995, private communication); and for the background source, T_0 = 233 K. For simplicity, we also took f_H, f_C, and X_{0C} equal to unity. The values of the fitted parameters are $T_H = 60 \pm 10$ K, $\tau_H(3, 3) = 0.55 \pm 0.05$; $\tau_C(3, 3) = 0.009 \pm 0.002$, and $X_{0H} = 0.12$; that is, the warm gas is mostly beside or behind the H II region.

The total column density of ammonia, derived from equation (3), is $\sim 3 \times 10^{16}$ cm^{-2}. Assuming an [H_2/NH_3] abundance ratio of 10^6, and a path length of 0.16 pc (0''.25 at the distance of 13 kpc), we derive a hydrogen molecular density of 5×10^4 cm^{-3}. The molecular mass, computed from equation (2) of Garay et al. (1993a), assuming LTE, an [H_2/NH_3] abundance ratio of 10^6, and $T_{bg} = 2.7$ K, is $\sim 18\ M_\odot$.

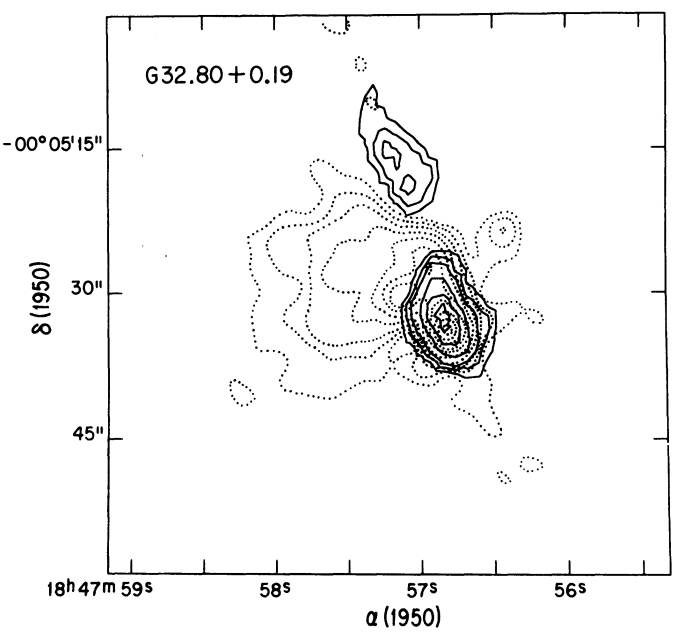

FIG. 10.—Contour map of the velocity-integrated emission in the (3, 3) line superposed on a contour map of the radio continuum map of G32.80+0.19 taken from Garay et al. (1994). Ammonia line contour levels are (−2, −1, 1, 2, 3, 5, 7, and 9) × 37 mJy beam^{-1} km s^{-1}. Radio continuum contour levels are −0.3, 0.3, 0.9, 2, 5, 10, 20, 30, 50, 70, and 90 percent of the peak brightness of 0.795 Jy beam^{-1}; the angular resolution is 2''.3 × 2''.2.

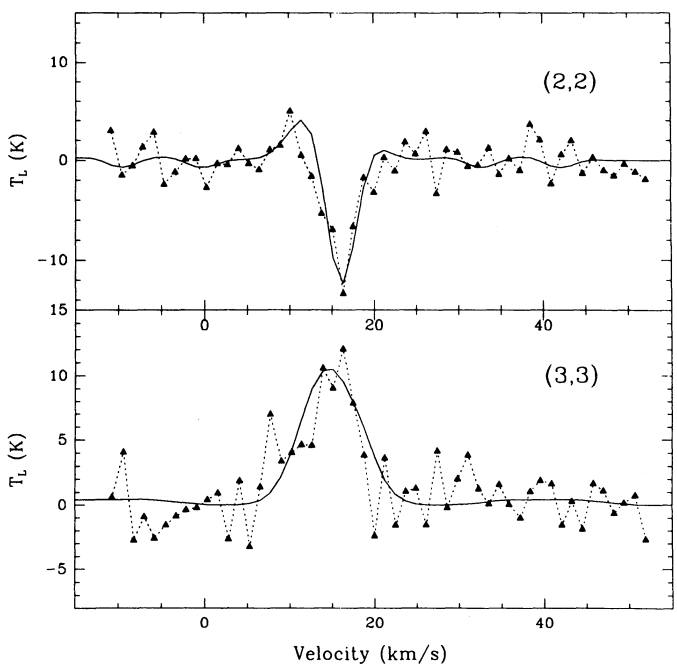

FIG. 11.—Spectra of the brightness temperature in the (2, 2) and (3, 3) NH_3 transitions observed at the peak position of the (2, 2) absorption feature from G32.80 South. The data are shown with black triangles; the solid line corresponds to the model discussed in the text (§ 4.1.3).

It is interesting to note that toward the G32.80+0.19 region, Plume et al. (1992) detected emission in the CS($J = 7$–6) line, having a line-center velocity of 15.5 km s^{-1} and a line width of 7.9 km s^{-1}. From the observed brightness temperature of the CS(7–6) line we derive, using their Figure 6, a lower limit for the molecular hydrogen density of 2×10^5 cm^{-3}, $\sim$4 times higher than the density derived from the ammonia observations. It is not clear, however, whether the high-density CS emission arises from the shocked molecular region associated with the cometary H II region or from the compact ammonia core associated with the compact H II region A, or both.

The questions arise as to the source of heating of the ammonia gas and the origin of the broad molecular line widths of the G32.80 South cloud. The primary candidate for the source of heating is radiation from the exciting star of the associated compact H II region, which has a luminosity of 3.5×10^5 $L_\odot$. Assuming that the dust in the NH_3 region is heated by the central star, we expect that at a distance of $\sim$0.1 pc (taking the radius of the continuum map; GLG), $T_{\rm dust} \sim 70$ K. If the dust and gas are well coupled by collision, the gas could be heated to a temperature $T_{\rm gas} \sim 60$ K, as observed in NH_3 (3, 3).

The observed line width in the (3, 3) line, of 7.1 km s^{-1}, is much broader than the thermal line width of 0.4 km s^{-1} expected for a kinetic temperature of $\sim$60 K, implying that nonthermal motions are dominant. Given the large magnitude of the line width, a turbulent contribution in the molecular gas is unlikely because it would be highly supersonic. A possible explanation that we consider, appraised by the similar line-center velocities of the ionized and molecular gas, is that the expansion of the associated compact H II region (source A) is driving a shock into the molecular gas accelerating it. The bulk velocity of expansion would broaden the line as observed. For the associated compact region of ionized gas, GLG measured, in the H92α line, a mean line-center velocity of 14.0 $\pm$ 0.4 km s^{-1} and a broad line width of $\sim$34 km s^{-1}, suggesting that the ionized gas is undergoing expansion motions. From the observed width in the (3, 3) line we estimate a shock velocity, V_s, of $\sim$7 km s^{-1} (see discussion in GLG, § 4.4.1). The molecular density of the ambient medium can then be obtained using the expression (cf. Spitzer 1978)

$$V_s^2 = C_{\rm II}^2 \frac{\rho_{\rm II}/\rho_{\rm I}}{1 - \rho_{\rm II}/4\rho_{\rm I}},$$

where $\rho_{\rm II}$ and $\rho_{\rm I}$ are the mass densities of the ionized and molecular regions, respectively, and $C_{\rm II}$ is the sound velocity in the ionized region. Using the electron density of the G32.80+0.19A compact H II region derived by GLG ($n_e \sim 2.7 \times 10^4$ cm^{-3}; $\rho_{\rm II} = 1.4 m_{\rm H} n_e$) and a sound speed in the ionized gas of $\sim$14.7 km s^{-1} (appropriate for $T_e \sim 16{,}000$ K; GLG), we find a molecular hydrogen density, $n(H_2)$, of $\sim 1 \times 10^5$ cm^{-3}. This estimate is $\sim$2 times larger than the value obtained from the ammonia observations (assuming $[H_2/NH_3] = 10^6$), but in agreement with the value derived from the observations of Plume et al. (1992). The shocked-gas hypothesis is not free of shortcomings, however. For instance, the height scale of the shocked layer is expected to be a small fraction ($\leq$5%) of the ionized radius (cf. Keto & Ho 1989). Our observations at 1.3 cm made with an angular resolution of $\sim$4″ show, however, that the ammonia cloud is $\sim$25% more extended than the compact H II region. Clearly, observations with higher angular resolution are needed to confirm (or deny) this possibility.

Another possibility is that the G32.80 South clump corresponds to a virialized primordial clump which has undergone the formation of massive stars in its central region. If one assumes virial equilibrium, from the observed radius of 0.08 pc and line width of 7.1 km s^{-1} we derive a total mass of $\sim$830 $M_\odot$. (Note that a similar mass is obtained assuming that the gas is collapsing toward the central stars.) From the total luminosity of $\sim 3.5 \times 10^5$ $L_\odot$, we know that there is at least one O-type star ionizing the region. It is not easy to determine how many and what type of stars are embedded in this clump. If we assume that the luminosity is produced from a stellar cluster that follows the initial mass function (IMF) of Miller & Scalo (1979), we found a large stellar density unlikely to occur in the small volume of ionized gas. Therefore, for simplicity, we correct only for the mass of an O6 ZAMS star which produces the 1.9×10^{49} s^{-1} of ionizing photons observed by GLG. The mass of molecular gas would then be $\sim$800 $M_\odot$, i.e., 40 times higher than the mass derived from the ammonia observations assuming an $[H_2/NH_3]$ abundance ratio of 10^6. To bring these two masses into agreement, we will need to adopt an abundance ratio of $\sim 4 \times 10^7$. Further studies are required to clarify this issue, and in this paper we will adopt $[H_2/NH_3] = 10^6$.

Finally, we note that the (2, 2) ammonia line width, of $\sim$3.5 km s^{-1}, is considerably larger than the thermal width expected for a kinetic temperature of 15 K, of $\sim$0.2 km s^{-1}, but is typical of the ammonia emission integrated over regions of $\sim$1 pc. For instance, in the survey of ammonia emission toward compact H II regions of Churchwell et al. (1990), made with an angular resolution of 40″, the average line width in the (2, 2) inversion transition is 3.4 $\pm$ 1.6 km s^{-1} (excluding the two largest values), and the average kinetic temperature is 28 K. The precise origin of the large nonthermal widths is not known. Possible explanations include motions of gas due to a large-scale collapse toward a central distribution of mass, motions due to the injection of momentum by the stellar winds from the stars exciting the H II regions, and magnetic turbulence.

4.2. *G61.48+0.09 Ammonia Clumps*

Single-dish mapping of the CO emission toward the G61.48+0.09 H II complex have been presented by Evans et al. (1981), Phillips et al. (1988), Phillips & Mampaso (1991), and White & Fridlund (1992). From CO observations, Evans et al. (1981) derived an average density at the core of the molecular cloud of $\sim 6 \times 10^3$ cm^{-3}. In addition, from the lack of observable H_2CO emission, they suggested that molecular clumps with high density ($\geq 10^5$ cm^{-3}) do not seem to be present. This conclusion is supported by the lack of detection of emission in the CS($J = 7 \rightarrow 6$) line toward this region (Plume et al. 1992). White & Fridlund (1992) found that the molecular gas in the core of the S88B cloud is distributed in a horseshoe-like structure around the H II regions, having a size of $\sim$1′, a kinetic temperature of 60 K, and a molecular mass of $\sim$400 $M_\odot$. Single-dish NH_3 observations, in the (1, 1) and (2, 2) inversion transition lines, show that the ambient molecular cloud toward G61.48+0.09 has an average velocity of $\sim$22.0 $\pm$ 0.3 km s^{-1} (Macdonald et al. 1981; Churchwell et al. 1990).

Our observations show that the dense ammonia gas toward G61.48+0.09 is intimately associated with the H II regions within this complex. This can be clearly appreciated in Figure 12, which shows the velocity-integrated emission in the (3, 3) ammonia line superposed on a contour map of the radio continuum emission at 8.3 GHz taken from GLG. Toward the east

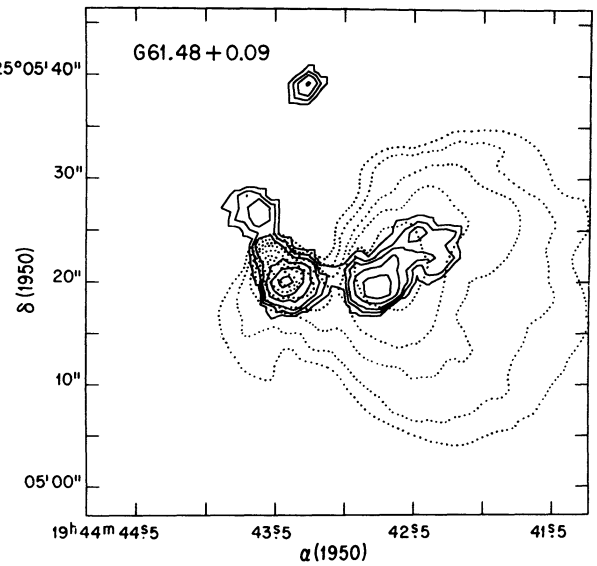

FIG. 12.—Contour map of the velocity-integrated emission in the (3, 3) line superposed on a contour map of the radio continuum map of G61.48+0.09 taken from Garay et al. (1994). Ammonia line contour levels are −20, −10, 10, 20, 30, 50, 70, and 90 percent of the peak brightness of 82.6 mJy beam^{-1} km s^{-1}. Radio continuum contour levels are −5, 5, 10, 20, 30, 50, 70, and 90 percent of the peak brightness of 0.154 Jy beam^{-1}; the angular resolution is 2".4 × 2".1.

and west clumps, the emission in the (3, 3) main HF line is relatively strong, while in the (2, 2) main HF line it is not (or is barely) detected, suggesting that the molecular gas is optically thin and warm. In what follows, we discuss in more detail the physical characteristics of the molecular clumps and their association with the compact H II regions.

4.2.1. *G61.48 East*

To determine the excitation temperature and optical depth of the warm gas, we modeled the observed profiles in the (2, 2) and (3, 3) transitions at the peak position of the G61.48 East clump, using the simple model (eq. [4]) described in § 4.1.3. At this position, the brightness temperature observed in the (3, 3) line is 7.6 K, and the brightness temperature of the radio continuum emision at 1.3 cm is 68 K. Figure 13 shows the observed spectra in the (2, 2) and (3, 3) transitions and the model spectra (*continuous line*) for the G61.48 East clump. The parameters of the model, taken from our observations, are, for the warm gas, $V_H = 21.9$ km s^{-1}, $\Delta v_H = 2.5$ km s^{-1}, and the background temperature, $T_0 = 68$ K; for the cold gas (taken from Churchwell et al. 1990), $V_C = 22.3$ km s^{-1} and $\Delta v_C = 2.6$ km s^{-1}.

Adopting $T_C = 15$ K (S. Kurtz 1995, private communication), a value that is in agreement with the lowest temperature estimate given by Evans et al. (1981), taking f_H, f_C, and X_{0C} equal to unity, and assuming that the warm ammonia clump is behind the H II region, the best fit to the observed spectra gave, for the warm cloud, $T_H = 70 \pm 15$ K and $\tau_H(3, 3) = 0.22 \pm 0.04$. The model emission expected in the (2, 2) line is of the order of our detection limits and is consistent with the observations. We note that the observed spectra can be equally well reproduced assuming that the ammonia clump is in front of the radio continuum source, in which case we derive $T_H \sim 140$ K. However, we argue below that the molecular gas is most likely behind the H II region.

Assuming $T_{ex} = T_{rot} \simeq 70$ K, and adopting a distance of 5.4 kpc (Churchwell et al. 1990), we derive a total ammonia column density of $\sim 6 \times 10^{15}$ cm^{-2}. Further, taking the minor axis as the angular size (1".5) and assuming an $[H_2/NH_3]$ abundance ratio of 10^6, we derive a molecular hydrogen density of 3×10^4 cm^{-3} and a molecular mass of $\sim 0.6\ M_\odot$.

The spatial distribution of the ammonia emission in the (3, 3) line from the G61.48 East clump is strikingly coincident with the compact region of ionized gas (component B2), which brings up the question of their physical association. The mean radial velocity of the emission in the (3, 3) line is 21.9 ± 0.2 km s^{-1}, close to the velocity of the ambient molecular gas and its FWHM line width of ~3.5 km s^{-1}. This small line width discards a shell geometry around the ionized gas observed by GLG; given the parameters of the ionized gas $n_e \sim 1.5 \times 10^4$ cm^{-3} and $\Delta v \sim 27$ km s^{-1}, and the molecular gas density inferred from the ammonia observations, $\sim 3 \times 10^4$ cm^{-3}, an expanding shell around this region would imply $\Delta v(NH_3) \sim 20$ km s^{-1}, i.e., much larger than the observed value. We suggest instead that this compact H II region is in the so-called champagne phase of its evolution, with the ionized gas being evacuated roughly in the direction toward the observer.

The ammonia emission probably arises from the molecular gas that is heated and compressed by the slow shock front moving in the direction of increasing density (away from the observer). The champagne hypothesis is supported by the radio recombination line profile of the ionized gas which shows, in Figure 2 of GLG, a blue wing due to the flow toward the observer. Also, in Figure 12 of GLG one can see that the head of the ionized gas has a velocity ~20 km s^{-1}, similar to the NH_3 velocity, with a gradient toward lower velocities. An estimate of the amount of gas expected to be contained in the compressed shocked layer can be obtained from equation (17) of Franco, Tenorio-Tagle, & Bodenheimer (1990). Assuming an ambient medium with constant density, equal to the density derived from the ammonia observations of 3×10^4 cm^{-3}, an exciting star with a rate of ionizing photons of 2.5×10^{48} s^{-1} (GLG) implying an initial Strömgren radius of 0.045 pc, and using the observed ionized radius of 0.071 pc, we derive a neutral mass in the shocked layer of 0.3 $M_\odot$, similar to the mass derived from the ammonia observations. In fact, Figure 14 shows a position-velocity diagram of the H92α recombination line data from GLG which shows an arclike shape, as expected for an outflow toward the observer.

4.2.2. *G61.48 West*

As for the G61.48 East ammonia clump, we determine the excitation temperature and optical depth using equation (4). The peak brightness temperature observed in the (3, 3) line is ≃7.5 K, and at this position the brightness temperature of the radio continuum is 42 K. Figure 13 shows the observed spectra in the (2, 2) and (3, 3) transitions and the model spectra (*continuous line*) for the G61.48 West clump. The parameters of the model taken from the observations are, for the warm gas, $V_H = 22.0$ km s^{-1} and $\Delta v_H = 2.1$ km s^{-1}; for the cold gas, $V_C = 22.3$ km s^{-1} and $\Delta v_C = 2.6$ km s^{-1} (Churchwell et al. 1990); and $T_0 = 42$ K. Adopting f_H, f_C, and X_{0C} equal to unity, and assuming that $T_C \simeq 15$ K and that the warm ammonia cloud is in front of the H II region, we derived, for the warm cloud, $T_H = 80 \pm 15$ K and $\tau_H(3, 3) = 0.28 \pm 0.06$. We considered the warm NH_3 cloud to be in front of the H II region because the ionized flow is redshifted.

Using $T_{ex} = T_{rot} \simeq 80$ K, we derive a total column density of

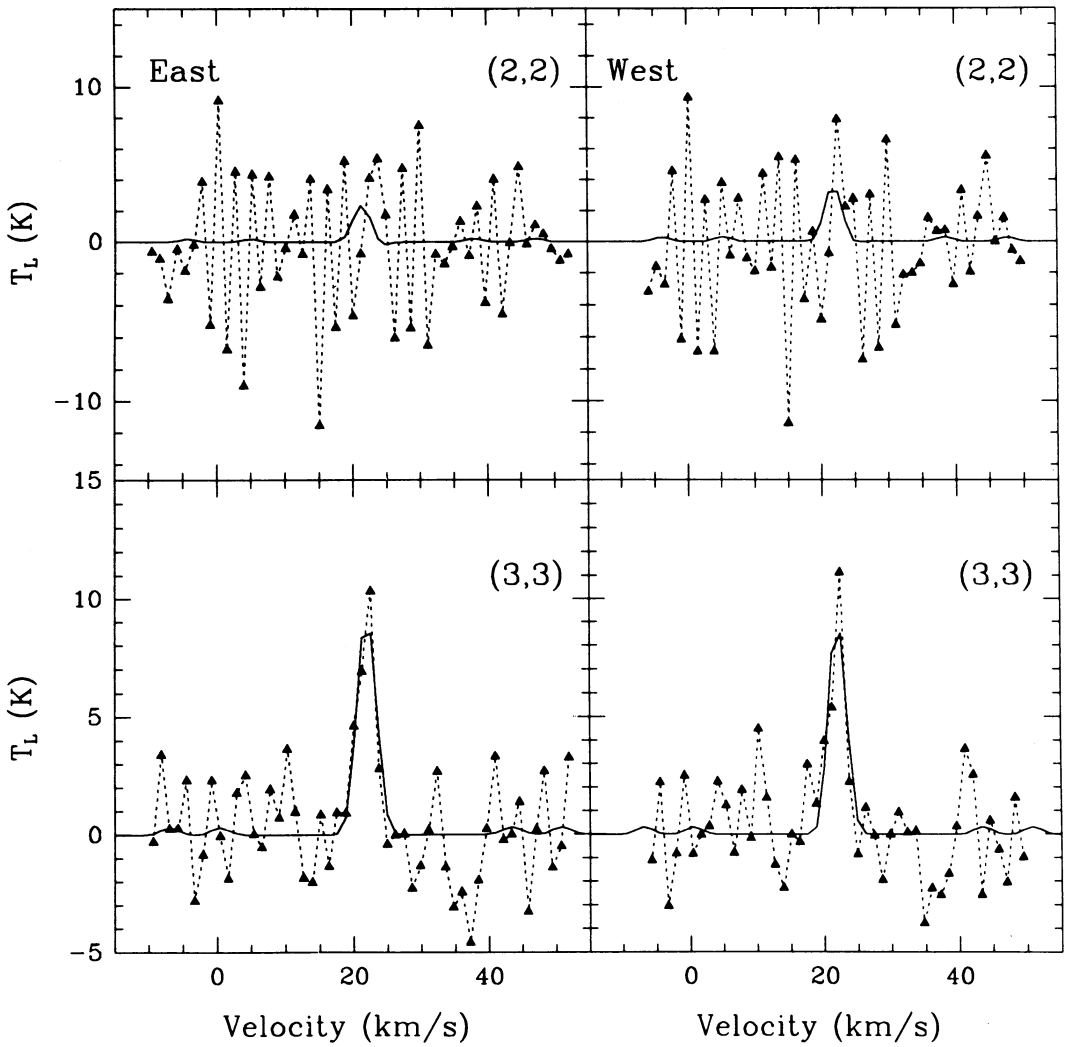

FIG. 13.—Spectra of the brightness temperature in the (2, 2) and (3, 3) NH_3 transitions observed at the peak position of the G61.48 East and G61.48 West ammonia clumps. The data are shown with black triangles; the solid line corresponds to the model discussed in the text (§ 4.2.1).

$\sim 1 \times 10^{16}$ cm^{-2}. Further, assuming an [H_2/NH_3] abundance ratio of 10^6, we derive a molecular hydrogen density of 4×10^4 cm^{-3} and a total molecular mass of $\sim 2\ M_\odot$.

Regarding the physical association between the compact molecular core and the cometary-like H II region, we note that the mean radial velocity of the ammonia gas in the (3, 3) main HF line is 21.6 ± 0.2 km s^{-1}, similar to the ambient molecular cloud velocity. On the other hand, GLG found that the velocity of the ionized gas at the head of the cometary H II region is ~ 21 km s^{-1}, increasing toward the tail, where it reaches ~ 33 km s^{-1}. The location of the dense ammonia gas toward the associated cometary region, roughly at the position of the head, and the similar velocities of the ammonia and H92α hydrogen lines at that position, strongly support the hypothesis that the ionized region is undergoing a champagne flow.

5. CONCLUSIONS

Using the VLA, we observed the G32.80+0.19 and G61.48+0.09 regions of star formation in the (2, 2) and (3, 3) inversion transitions of ammonia. These sources contain cometary-like compact and ultracompact H II regions. The main results and conclusions presented in this paper are summarized as follows.

5.1. *G32.80+0.19*

Toward the G32.80+0.19 region we found that the ammonia emission arises from three distinct and compact structures: G32.80 North, G32.80 Middle, and G32.80 South. The G32.80 North ammonia structure, seen in emission in the main HF line of the (2, 2) and (3, 3) inversion transitions, has a size of 0.7 × 0.1 pc and is located just beyond and roughly following the northwestern edge of the cometary H II region. It has a mean line-center velocity of ~ 18.6 km s^{-1}, redshifted with respect to the ambient molecular cloud by 2.3 km s^{-1}. We estimated that the molecular gas in this clump has a rotational temperature of 56 K, a hydrogen density of 9×10^3 cm^{-3}, and a mass of $\sim 10\ M_\odot$. The G32.80 Middle clump is detected in absorption in the (2, 2) main HF line and in emission in the (3, 3) main HF line. The absorption feature appears projected just on top of the head of the cometary region of ionized gas, and has a radial velocity of ~ 17 km s^{-1}. We suggest that this feature arises in the low-density, low-temperature, ambient molecular gas that surrounds the H II regions, which has a

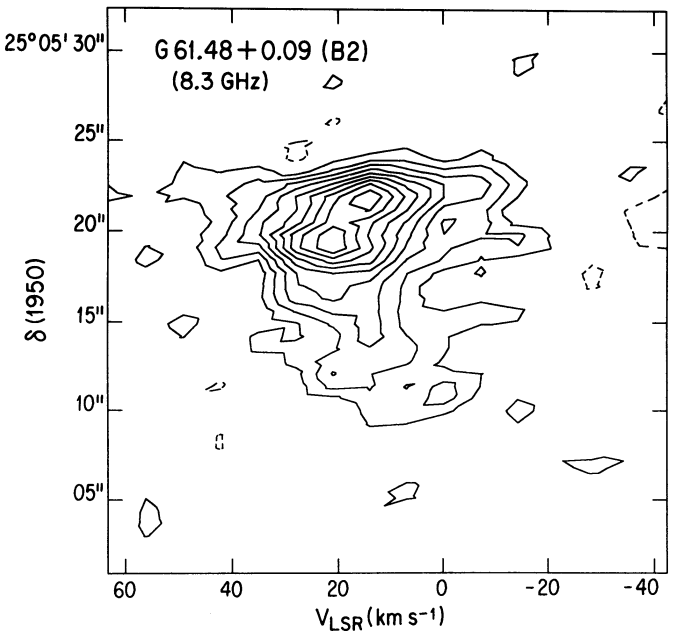

FIG. 14.—Position-velocity diagram of the H92α recombination line toward G61.48 East. The data were taken from Garay et al. (1994). The cut was made along the north-south direction passing through $\alpha = 19^h44^m43^s.7$. Contour levels are −10, 10, 20, 30, 40, 50, 60, 70, 80, and 90 percent of the peak brightness of 6.48 mJy beam^{-1}. This figure shows an arclike shape, as expected for an outflow toward the observer.

mean velocity of ~16.3 km s^{-1}. The (3, 3) emission feature, slightly displaced toward the west of the absorption feature, closely follows the outer edge of the head of the cometary H II region and has a velocity of ~15 km s^{-1}. We suggest that the ammonia emission from the middle clump arises in the post-shock layer of warm gas behind the shock front driven by the expansion of the H II region into the molecular gas. The similar velocities of the ammonia gas and of the ionized gas at the head position, together with the smooth increase in the velocity of the ionized gas (from ~14 km s^{-1} at the head's leading edge to ~22 km s^{-1} at the tail's edge; GLG), being in a direction opposite to the direction of increasing molecular density, as established from the present ammonia observations, strongly support the idea that this cometary-like H II is undergoing a champagne flow. Toward the G32.80 South ammonia clump, which has a size of ~0.2 pc, the (2, 2) main HF line exhibits both absorption and relatively weak emission, while the (3, 3) main HF line appears only in emission. We found that it is possible to reproduce the observed spectra assuming that there is a blend, within a synthesized beam, of an emitting region of warm molecular gas and an absorbing region of cold gas in front of a continuum source. For the warm gas we derived an excitation temperature of 60 K, a molecular hydrogen density of 5×10^4 cm^{-3}, and a total molecular mass of 18 $M_\odot$. The emission in the (3, 3) line has an average center velocity of 14.1 km s^{-1}, similar to the mean velocity of the ionized gas of the associated H II region, and a line width of 7.1 km s^{-1}. We suggest that the broad line width is due to motions of the molecular gas produced by the expansion of the associated compact H II region into the molecular clump.

5.2. *G61.48+0.09*

Our high angular resolution observations show that the ammonia emission, in the main HF line of the (3, 3) inversion transition, from the G61.48+0.09 complex arises from two small clumps whose peak positions lie close to the peak position of the regions of ionized gas. The G61.48 East ammonia clump is spatially coincident with the compact H II region B2. It has a mean radial velocity of ~21.9 km s^{-1}, similar to the velocity of the ambient molecular cloud. We argue that the molecular gas from the east component is behind the compact H II region, so the ionized gas is undergoing a champagne flow toward the observer. We derive an excitation temperature of ~70 K, a molecular hydrogen density of $\sim 3 \times 10^4$ cm^{-3}, and a total molecular mass of 0.6 $M_\odot$. The G61.48 West ammonia clump is located close to the head of the cometary H II region B1 and has a radial velocity of ~21.6 km s^{-1}. The observed location and velocity of the ammonia clump, together with the fact that the mean velocity of the ionized gas increases from ~21 km s^{-1} at the head structure to ~33 km s^{-1} in the tail's region, strongly support the hypothesis that this cometary H II region is undergoing a champagne flow. For the G61.48 West ammonia clump we derived an excitation temperature of ~80 K, a molecular hydrogen density of $\sim 4 \times 10^4$ cm^{-3}, and a total molecular mass of ~2 $M_\odot$.

Y. G. and S. L. acknowledge support from grants DGAPA-UNAM IN100793 and CONACyT 4916-E9406. G. G. gratefully acknowledges support from a Guggenheim Fellowship and from the Chilean FONDECYT project 0907-92. We also appreciate fruitful discussion with L. F. Rodríguez and S. Kurtz.

REFERENCES

Bodenheimer, P., Tenorio-Tagle, G., & Yorke, H. W. 1979, ApJ, 233, 85
Churchwell, E., Walmsley, C. M., & Cesaroni, R. 1990, A&AS, 83, 119
Evans, N. J., II, Blair, G. N., Harvey, P., Israel, F., Peters, W. L., III, Scholters, M., De Graaum, T., & Vanden Bout, P. 1981, ApJ, 250, 200
Felli, M., & Harten, R. H. 1981, A&A, 100, 42
Fey, A. L., Claussen, M. J., Gaume, R. A., Nedoluha, G. E., & Johnston, K. J. 1992, AJ, 103, 234
Franco, J., Tenorio-Tagle, G., & Bodenheimer, P. 1990, ApJ, 349, 126
Garay, G., Lizano, S., & Gómez, Y. 1994, ApJ, 429, 268 (GLG)
Garay, G., Moran, J. M., & Rodríguez, L. F. 1993a, ApJ, 413, 582
Garay, G., & Rodríguez, L. F. 1990, ApJ, 362, 191
Garay, G., Rodríguez, L. F., Moran, J. M., & Churchwell, E. 1993b, ApJ, 418, 368
Genzel, R., Downes, D., Ho, P. T. P., & Beiging, J. 1982, ApJ, 259, L103
Hofner, P., & Churchwell, E. 1995, in preparation
Keto, E. R., & Ho, P. T. P. 1989, ApJ, 347, 349
Kurtz, S., Churchwell, E., & Wood, D. O. S. 1994, ApJS, 91, 659
Kurtz, S., Churchwell, E., Wood, D. O. S., & Myers, P. 1995, in preparation
Macdonald, G. H., Little, L. T., Brown, A. T., Riley, P. W., Matheson, D. N., & Felli, M. 1981, MNRAS, 195, 387
Mac Low, M.-M., Van Buren, D., Wood, D. O. S., & Churchwell, E. 1991, ApJ, 369, 395
Miller, G. E., & Scalo, J. M. 1979, ApJS, 41, 513
Miralles, M. P., Rodríguez, L. F., & Scalise, E. 1994, ApJS, 92, 173
Phillips, J. P., et al. 1988, A&A, 190, 289
Phillips, J. P., & Mampaso, A. 1991, A&AS, 88, 189
Plume, R., Jaffe, D. T., & Evans, N. J., II. 1992, ApJS, 78, 505
Schwab, F. 1980, Proc. SPIE, 231, 18
Spitzer, L. 1978, Physical Processes in the Interstellar Medium (New York: Wiley)
Tenorio-Tagle, G. 1979, A&A, 71 59
Van Buren, D., & Mac Low, M.-M. 1992, ApJ, 394, 534
Van Buren, D., Mac Low, M.-M., Wood, D. O. S., & Churchwell, E. 1990, ApJ, 353, 570
White, G. J., & Fridlund, C. V. M. 1992, A&A, 266, 452
Wood, D. O. S., & Churchwell, E. 1989, ApJS, 69, 831
Yorke, H. W., Tenorio-Tagle, G., & Bodenheimer, P. 1984, A&A, 138, 325